Ice nucleating properties of the sea ice diatom *Fragilariopsis cylindrus* and its exudates

Lukas Eickhoff[1], Maddalena Bayer-Giraldi[2,a], Naama Reicher[3], Yinon Rudich[3], Thomas Koop[1]

[1]Faculty of Chemistry, Bielefeld University, Universitätsstraße 25, 33615 Bielefeld, Germany
[2]Faculty of Mathematics, Informatics and Natural Sciences, Universität Hamburg, 20354 Hamburg, Germany
[3]Department of Earth and Planetary Sciences, Weizmann Institute of Science, 76100 Rehovot, Israel
[a]formerly at: Alfred Wegener Institute, Helmholtz Centre for Polar and Marine Research, 27568 Bremerhaven, Germany

Correspondence to: Thomas Koop (thomas.koop@uni-bielefeld.de)

Supplemental Information

Differential scanning calorimetry experiments

The principle preparation procedure for the water-in-oil emulsion (w/o) samples was almost identical to the method described earlier (Dreischmeier et al., 2017). 1 mL of 7 wt% emulsifier Span®65 (Merck) dissolved in 93 wt% of a mixture of 50 vol% methylcyclopenthane (Acros Organics, 99 %) and 50 vol% methylcyclohexane (Acros Organics, 95 %) was used as the organic phase. The aqueous phase consisted of 1 mL of an *F. cylindrus* suspension with a concentration of 1×10^7 cells mL^{-1}, see Sect. 2.2.2 in the main paper, or alternatively of 1 mL of pure artificial seawater for comparison. The mixtures of the organic and aqueous phase were subsequently emulsified by stirring with a high-speed disperser (IKA Ultra-Turrax T25 basic) for 10 min at 20'000 rpm. For a DSC measurement, about 10 mg of such an emulsion was filled into an aluminium pan that was sealed hermetically and then transferred into the calorimeter. The samples were cooled at a rate of -5 °C min^{-1} down to -60 °C, and subsequently reheated, first at 5 °C min^{-1} and then, in the temperature range between -20 °C and +5 °C, at 1 °C min^{-1}.

WISDOM microfluidic device

For the droplet generation, we used two syringe pumps (neMESYS NEM-B101-02 E), one filled with the aqueous sample and another with an organic phase consisting of 2 wt% Span®80 (Merck) dissolved in 98 wt% of a mineral oil (Sigma-Aldrich, mineral oil M3516). The microfluidic chip was connected to the pumps with PTFE tubes. The droplets generated within the chip had diameters of 90 µm ±5 µm.

For the freezing experiments, we placed the microfluidic chip after the droplet production on a temperature-controlled cold-stage (Linkam, BCS 196) attached to an optical microscope (Olympus, BX51 TRF). The temperature of the droplets in the chip was calibrated with respect to the cooling (or heating) rate as well as to the absolute temperature, and is described in detail in a previous study (Eickhoff et al., 2019). The freezing of the droplets was observed using the transmission mode of the microscope and we recorded the images with a digital camera (Q-Imaging, MicroPublisher 5.0 RTV) for later analysis by a LabView routine that detects a freezing event from the change in grey values of a particular droplet upon freezing. Typical changes in the droplets' grey values during freezing experiments are depicted in Fig. S3. In each individual experiment, between about 45 to 70 droplets were observed simultaneously, depending upon the percentage of droplet-filled microcells within the droplet array of the chip.

For all *F. cylindrus* measurements, the chip was first cooled to a temperature of -20 °C at a rate of -5 °C min^{-1}, because no freezing events were detected in this temperature range. After equilibration at this temperature for 2 min, the samples were then cooled at a slower rate of -1 °C min^{-1} to -45 °C, at which all droplets were frozen. Thereafter, the chip was heated relatively quickly at a rate of 5 °C min^{-1}, until -10 °C, and after two minutes of equilibration, it was then heated to 5 °C at 1 °C min^{-1}. The detailed temperature profiles for each type of experiment are listed in Table S2.

Evaluation procedure for samples with small INP concentrations

Referring to section 2.3.3 in the main paper, the following Poisson distribution can be used to describe the probability $P_\lambda(k)$ that an individual droplet contains exactly k INPs when the average concentration is λ INPs per droplet:

$$P_\lambda(k) = \frac{\lambda^k}{k!}\exp(-\lambda). \tag{S1}$$

Note that the derivation of the Poisson distribution contains a simplification that require a larger number of droplets and hence Eq. (S1) becomes more accurate as the number of investigated droplets increases. For the microfluidic experiments performed in this work with more than a hundred droplets investigated for each sample the simplification applies.

The average number of INPs per droplet, λ, is easily calculated from the concertation c of INPs in the stock solution and the volume V of an individual microfluidic droplet:

$$\lambda = c \cdot V_{\mathrm{drop}}. \tag{S2}$$

Furthermore, the droplet volume V_{drop} can be expressed by the droplet's radius r or alternatively by its diameter d:

$$V_{\mathrm{drop}} = \frac{4}{3}\pi \cdot r^3 = \frac{1}{6}\pi \cdot d^3. \quad \text{(S3)}$$

Figure S4 shows the calculated Poisson distributions of the number of cells per droplet for four different values of λ in a concentration range relevant to this study. For lower values of λ, the histograms exhibit the tilted shape typical of Poisson distributions, while for larger values of λ, the Poisson distribution approaches the more symmetrical shape of a normal distribution (Koop et al., 1997).

For the ice nucleation experiments considered here, only those droplets containing at least one INP and those without any INPs are relevant, as this determines whether they are subject to heterogeneous or homogeneous nucleation, respectively. Whether a droplet contains one, two or more INPs is of less importance, as long as every INP is identical and, thus, induces heterogeneous ice nucleation at the same temperature. The probability that a droplet does not contain any INPs can be calculated easily by inserting $k = 0$ into Eq. (S1):

$$P_\lambda(0) = \frac{\lambda^0}{0!}\exp(-\lambda) = \frac{1}{1}\exp(-\lambda) = \exp(-\lambda). \quad \text{(S4)}$$

$P_\lambda(0)$ is shown as the black-coloured bar in each panel of Fig. S4. The probability that a droplet contains at least one INP, $P_\lambda(k \geq 1)$, is given by the combined probability of all red-coloured bars in each panel of Fig. S4, and it can be calculated using the fact that the sum of all probabilities $P_\lambda(k)$ for k from 0 to ∞ must become 1 (see Eq. (S5)):

$$P_\lambda(k) = \sum_{k=0}^{\infty} \frac{\lambda^k}{k!}\exp(-\lambda) = 1. \quad \text{(S5)}$$

Hence, $P_\lambda(k \geq 1)$ can be calculated from the following difference:

$$P_\lambda(k \geq 1) = \sum_{k=1}^{\infty} \frac{\lambda^k}{k!}\exp(-\lambda) = \sum_{k=0}^{\infty} \frac{\lambda^k}{k!}\exp(-\lambda) - \sum_{k=0}^{0} \frac{\lambda^k}{k!}\exp(-\lambda) = 1 - P_\lambda(0) = 1 - \exp(-\lambda). \quad \text{(S6)}$$

Since λ can be expressed by the product of the droplets' diameter and the known concentration of INPs in the stock solution, c, (see Eq. (S2) and Eq. (S3)) this yields:

$$P_\lambda(k \geq 1) = 1 - \exp\left(-\frac{\pi}{6} \cdot c \cdot d^3\right). \quad \text{(S7)}$$

The equations above have been derived for applications where the average concentration c of INPs in solution is known. However, in ice nucleation experiments of natural samples, the concentration c of INPs per volume is often unknown a priori and other values such as the organic carbon content has to be used for comparison (Gute and Abbatt, 2020; Xi et al., 2021). In such cases, Eq. (S7) can be used to obtain a rough estimate of λ and, thus, c from ice nucleation experiments when a plateau in the experimental frozen fraction curve is observed. The frozen fraction is defined as the number of frozen droplets relative to the number of all droplets, at a given temperature (Budke and Koop, 2015). Here, we term the value of the frozen fraction at the plateau as f'_{ice}. If a sufficiently large number of droplets is investigated, then f'_{ice} corresponds to the fraction of droplets that froze heterogeneously and thus may be equated with that fraction of droplets containing at least one INP.

There are two underlying assumptions for experimentally obtaining f'_{ice}. First, every droplet containing at least one INP freezes heterogeneously, which appears entirely reasonable. Secondly, every droplet containing one or more INPs freezes at a higher temperature than those droplets without any INP, i.e. the difference between the heterogeneous and homogeneous ice nucleation temperature is large enough to be easily distinguished in the experiment. With these two assumptions a plateau in the frozen fraction curve can be interpreted as follows: the fraction of droplets below the plateau froze heterogeneously and contain at least one INP, and the fraction of droplets above the plateau froze homogenously (when their freezing temperature is consistent with homogenous freezing) and, thus, do not contain INPs. In practice, this evaluation procedure does not work if none of the droplets froze heterogeneously or if all droplets froze heterogeneously at the same temperature without any obvious plateau, i.e. it is only applicable for intermediate average INP concentrations in what we term the "Poisson relevant range".

We define this "Poisson relevant range" as the range of average INP concentrations, in which both droplets without any INP as well as droplets containing one or more INPs occur and, thus, both can be observed readily in the corresponding freezing experiments. For the experiments presented here, we establish the Poisson relevant range as the area between $P_\lambda(k \geq 1)$ values of 5.0 % and 99.5 %. The lower limit was set at 5.0% in order to avoid any influence of the freezing of a minor fraction of droplets induced by impurities and the upper limit corresponds to about one out of 200 droplets not containing any INP and thus freezing homogeneously, while the highest accuracy can be reached for a value of 50 % (see blue curve in Fig. S5a and Fig. S6). For higher concentrations, when every droplet contains at least one INP, the above Poisson evaluation is not needed and the classic method can be used, and so this upper limit sets an endpoint for the Poisson-based evaluation. The classic method indeed assumes that every observed droplet contains at least one INP and it has been described in detail previously (Murray et al., 2012; Budke and Koop, 2015).

To demonstrate the concentration range suitable for the Poisson method, i.e. the Poisson relevant range, the latter is indicated in Fig. S5a as the grey shaded area. The solid blue curve shows the values of $P_\lambda(k \geq 1)$ calculated using Eq. (S7) as a function of the average INP concentration c of the studied sample and a droplet diameter of 90 µm. The two dashed lines show the changes for a deviation of ±5 µm in droplet diameter.

To verify the procedure, we investigated aqueous suspensions of the well-studied ice-nucleating bacterium *Pseudomonas syringae* in the form of the commercial product Snomax (Morris et al., 2011; Budke and Koop, 2015; Wex et al., 2015). The ice nucleation temperatures of each about 165±15 droplets, from three single measurements with 45 to 70 droplets each, containing either pure double-distilled water or three different concentrations of *P. syringae* were investigated, see Table S3. These concentrations are also marked in Fig. S5a as vertical lines. A similar plot for the *F. cylindrus* diatoms can be found in Fig. S6. The resulting experimental frozen fraction curves of *P. syringae* are shown in Fig. S5b. Double-distilled water (black open symbols) shows a steep increase in frozen fraction below about -34.0 °C, in agreement with homogeneous ice nucleation rates of droplets of such diameter (Koop and Murray, 2016; Reicher et al., 2018; Eickhoff et al., 2019). Following this observation, all droplets of the *P. syringae* samples that froze at around or below this temperature are assumed to have nucleated homogenously, i.e. they are considered to contain no INPs in the analysis below.

For all *P. syringae* samples, the first freezing events occur at much higher temperatures of about -8 to -9 °C, and the frozen fraction curve in each case initially increases strongly before reaching a plateau, and subsequently the remaining liquid droplets freeze only at very low temperatures. In each sample, the plateau occurs at a different value of the frozen fraction, e.g. f'_{ice} is higher the larger the *P. syringae* concentrations (pink > blue > orange). We determined the corresponding f'_{ice} values, as defined above, from the experimentally obtained frozen fraction curve as the value of the frozen fraction at -34.0 °C, i.e. at the threshold between heterogeneous and homogenous ice nucleation as defined above. The resulting f'_{ice} values for the three concentrations were 0.99, 0.61, and 0.39, respectively, indicated as the dashed horizontal lines in Fig. S5b. These f'_{ice} values correspond to $P_\lambda(k \geq 1)_{\mathrm{measured}}$ and can be used to infer the average INP concentration from Eq. (S7). Because in the current experiments the INP concentrations are known (i.e., $1.4\mathrm{x}10^7$, $2.8\mathrm{x}10^6$. and $1.4\mathrm{x}10^6$ mL^{-1}), these experimentally derived f'_{ice} values can be compared to the expected f_{ice} values, corresponding to $P_\lambda(k \geq 1)_{\mathrm{calcualted}}$ values calculated from Eq. (S7), yielding values of 1.00±0.01, 0.66±0.06 and 0.41±0.05, respectively. These theoretical values are in good agreement (within experimental uncertainty) with the measured values and thus confirm our approach and the inferred INP concentrations of $1.2\mathrm{x}10^7$, $2.5\mathrm{x}10^6$ and $1.3\mathrm{x}10^6$ mL^{-1} (see Table S3) deviate by about 14%, 11% and 7% from the prepared concentrations, which is very good given that INP concentrations can vary by orders of magnitude. For further validation that the Poisson distribution is necessary for a proper evaluation in the above-mentioned concentration range, the cumulative number of active ice-nucleating sites n_N per number of *P. syringae* bacteria was evaluated and discussed in the following section and the related Fig. S7.

Determination of INP concentration

Above, we have defined $f_{ice}^{'}$ as the plateau region separating heterogeneous and homogenous freezing. Since $f_{ice}^{'}$ varies with the number of droplets containing at least one INP, an experimentally determined $f_{ice}^{'}$ value can be used to calculate the concentration of INPs for unknown samples using a variation of Eq. (S7). Typically, a sample is investigated by means of a dilution series so that a different INP concentration is scanned in each experiment. If the INP concentration is too large, all droplets freeze heterogeneously, and if it is too low, no INP-induced heterogeneous nucleation occurs (apart from that induced by any impurity present) and, thus, all droplets freeze homogeneously. In both these cases, it is not possible to obtain the desired INP concentration. But if measurements are done in the Poisson relevant concentration range, one can observe both heterogeneous as well as homogenous freezing of droplets, resulting in a plateau in the frozen fraction curve, as discussed above. With the frozen fraction value of this plateau, $f_{ice}^{'}$, and the assumptions that, first, every INP induces heterogeneous freezing and that, secondly, all heterogeneously frozen droplets freeze before the first freezing of a homogenous frozen droplet, the following equation can be obtained by rearranging Eq. (S7):

$$c = -\frac{6\ln(1-P_\lambda(k\geq 1))}{\pi \cdot d^3} = -\frac{6\ln(1-f_{ice}')}{\pi \cdot d^3}. \quad \text{(S8)}$$

A comparison with Fig. S5a implies that $f_{ice}^{'}$ values of about 0.5 will lead to more accurate results than values close to the limits of the Poisson relevant range, because of the larger slope of the curve at $P_\lambda(k \geq 1)$ at intermediate $f_{ice}^{'}$ values.

In order to verify this method, we determine the concentrations c_{measured} of the investigated *P. syringae* samples by using the already determined values of $P_\lambda(k \geq 1)_{\text{measured}}$, from Table S3, for calculating $f_{ice}^{'}$. The resulting values for c_{measured} as well as the actually prepared concentrations of the samples c, are also listed in Table S4. The comparison shows that there are only minor differences between the prepared and measured concentrations, supporting the fact that this method provides a suitable and relatively accurate estimate of the INP concentration of an unknown sample. A similar treatment was performed for the *F. cylindrus* diatom samples and the related Fig. S6.

Figure S7 shows the cumulative number of ice-nucleating active sites n_N per *P. syringae* cell. As we will see below, the Poisson evaluation is required for this type of evaluation. The cumulative number of active ice-nucleating sites is given formally by Eq. (S9) (Budke and Koop, 2015):

$$n_N = \frac{-\ln(1-f_{ice})}{c \cdot V}. \quad \text{(S9)}$$

Here, f_{ice} is the frozen fraction, c is the INP concentration in absolute number of INPs per volume unit (i.e., the number density), and V is the volume of each individual droplet.

Figure S7 shows that for temperatures lower than about -35 °C, n_N obtains values that are larger than one per bacterium cell, implying that one bacterium initiates ice nucleation in more than one droplet, which is of course unreasonable. Instead, these high n_N values result from homogenous ice nucleation in droplets that do not contain any *P. syringae* bacteria, which normally is not considered in the classical n_N evaluation. By applying Eq. (S7) on these measurements, the threshold value between droplets that do contain INPs and those that do not can be determined. This treatment results in maximum values for n_N of about one per bacterial cell, as indicated by the filled and open circles in Fig. S7.

Results of the DSC experiments

For the DSC measurements, an inverse emulsion of pure artificial seawater as a reference was compared with an emulsion of artificial seawater containing 1×10^7 *F. cylindrus* cells mL^{-1}, see Fig. S8. First, the endothermic ice melting signals of the reference and the sample in Fig. S8a show almost the same signal, indicating that any colligative effect of the diatoms is negligible when compared to the amount of the dissolved ions in the artificial seawater. This similarity in the ice melting signals also implies no change in water activity of the artificial seawater upon the addition of the diatoms and, thus, no colligative effect on the homogeneous ice nucleation (freezing) signals is to be expected

The exothermic freezing signals for both emulsions are shown in Fig. S8b. For the seawater reference, one distinct nearly symmetrical freezing signal is revealed with a maximum at about -44 °C and an onset, which is defined as the freezing temperature of the sample, at about -40 °C. In contrast, the *F. cylindrus* sample shows the same maximum, but in addition a second exothermic signal in the form of a shoulder at about -42 °C, with an onset at a somewhat higher temperature of -39 °C when compared to the reference, and with small signals as high as -34 °C. Because of the colligative freezing point depression of the seawater, the freezing temperatures of the reference and the sample are shifted to lower temperatures, compared to pure water.

The larger broad signal in both emulsion samples corresponds to the homogeneous ice nucleation temperature of artificial seawater. This signal is also observed in the *F. cylindrus* sample because many of the emulsion droplets in that sample do not contain diatoms. The exothermic shoulder of the signal, which is not present in the reference, is most likely due to the freezing of droplets containing a diatom cell or fragment, and the shift of the onset to higher temperature is a first indication for the heterogeneous ice nucleation activity of the diatoms.

Because of the fact that the diatoms are of similar size as the emulsion droplets and the potential of mechanical disruption of diatom cells during the fast stirring of the disperser during emulsion preparation, these emulsion experiments appear to us as not suitable for a quantitative analysis of the ice nucleation activity of *F. cylindrus*. Thus, we employed non-invasive methods in the experiments described below.

Parametrization of *F. cylindrus* ice nucleation efficiency

In Eq. (2) in the main paper, we provide a parametrization representing the ice nucleation of the different sea ice diatoms in shown in Fig. 7 of the main paper in terms of the number of ice active sites per total mass of diatom cells, n_{m_total}. We also derived a parametrization for the individual ice nucleation efficiency of the *F. cylindrus* diatoms (see Fig. S9), which is given in the following Eq. (S10):

$$\log_{10}(n_{m\_\mathrm{total}}\ \mathrm{g}^{-1}) = -0.521789°\mathrm{C}^{-1} \cdot T - 6.1761. \quad \text{(S10)}$$

where T is temperature to be entered in units of °C. For numerical code verification, Eq. (S10) should result in a value for n_{m_total} of 8.2x10^7 g^{-1} at a temperature of -27.0 °C. This parametrization is valid over the temperature range between -24.5 °C to -34.5 °C.

Table S1: Salts used for the preparation of artificial seawater for the *F. cylindrus* ice nucleation experiments. The amounts of substances provided for each ion yield a mass of 500 g artificial seawater at a salinity of 34.5.

Salt	Supplier	m [g]	Na^+ [mmol]	K^+ [mmol]	Mg^{2+} [mmol]	Ca^{2+} [mmol]	Cl^- [mmol]	SO_4^{2-} [mmol]	H_2O [mmol]
NaCl	VWR Chemicals	11.8446	202.68				202.68		
KCl	VWR Chemicals	0.3758		5.04			5.04		
$MgCl_2 \cdot 6H_2O$	ITW Reagents	5.3280			26.21		52.42		157.25
$Na_2SO_4 \cdot 10H_2O$	Acros Organics	4.4902	27.87					13.94	139.36
$CaCl_2 \cdot 2H_2O$	ITW Reagents	0.7460				5.07	10.15		10.15
H_2O	double distilled water	477.23							26490.26
artificial seawater		**500.01**	**230.55**	**5.04**	**26.21**	**5.07**	**270.28**	**13.94**	**26797.02**

Table S2: Temperature parameters used in the microfluidic freezing experiments. The first number in each triplet is the final temperature of the respective step in °C, the second number indicates the rate of cooling or heating in °C min^{-1}, and the third number indicates the holding time at the final temperature in min. Reference samples were always investigated with the same parameters as those given for each sample.

Step	*F. cylindrus*	*F. cylindrus* (filtered)	*F. cylindrus* (pure cells)	*F. cylindrus* (Medium)	*fc*IBP11	*P. syringae*
1	-20/-5/2	-20/-5/2	-20/-5/2	-20/-5/2	-20/-5/2	-5/-5/2
2	-45/-1/0	-45/-1/0	-45/-1/0	-45/-1/0	-45/-1/0	-40/-1/0
3	-10/5/2	-10/5/2	-10/5/2	-10/5/2	-10/5/2	-10/5/2
4	5/1/0	5/1/0	5/1/0	5/1/0	5/1/0	5/1/0

Table S3: As prepared concentrations $\boldsymbol{c}$ of the *P. syringae* samples, calculated fractions of droplets with at least one bacterium $\boldsymbol{P_\lambda(k \geq 1)}_{\text{calculated}}$, as well as measured fractions $\boldsymbol{P_\lambda(k \geq 1)}_{\text{measured}}$ and experimentally determined concentrations $\boldsymbol{c}_{\textbf{measured}}$ based on the approach outlined above using Eq. (S8).

$\boldsymbol{c}$ / mL^{-1}	$\boldsymbol{P_\lambda(k \geq 1)}$ calculated	$\boldsymbol{P_\lambda(k \geq 1)}$ measured	$\boldsymbol{c}$ measured / mL^{-1}
1.4x10^7	$1.00^{+0.00}_{-0.01}$	0.99	1.2x10^7
2.8x10^6	$0.66^{+0.06}_{-0.06}$	0.61	2.5x10^6
1.4x10^6	$0.41^{+0.05}_{-0.05}$	0.39	1.3x10^6

Table S4: Shifts in ice nucleation temperature relative to the ΔT_{50} of artificial seawater for the untreated *F. cylindrus* samples, as well as for the samples filtered with a 0.22 µm syringe filter.

c	unfiltered ΔT_{50}	filtered ΔT_{50}
$5x10^7$ mL^{-1}	7.2 °C	6.4 °C
$1x10^7$ mL^{-1}	6.0 °C	5.2 °C
$2x10^6$ mL^{-1}	5.4 °C	3.1 °C
$1x10^6$ mL^{-1}	4.8 °C	2.6 °C
$5x10^5$ mL^{-1}	2.8 °C	0.0 °C

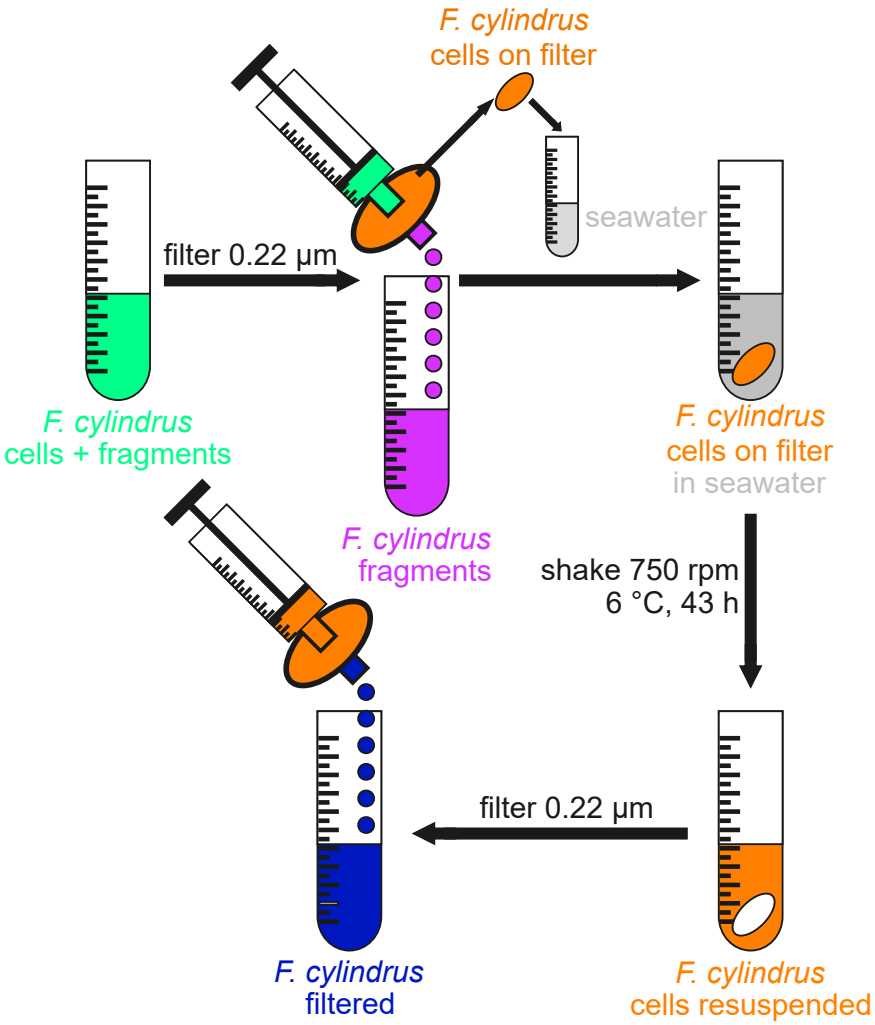

Figure S1: Extraction of the pure *F. cylindrus* cells by filtration of the stock solution (green). After filtration, the filtrate (purple) should only contain smaller cell fragments and soluble molecules such as *fc*IBP, while whole cells and larger fragments remain on the filter (orange filter). By shaking the filter in artificial seawater (grey), the cells were resuspended (orange solution). As a finally test, filtration of this suspension (blue) should not show any ice nucleation results different from those of pure artificial seawater.

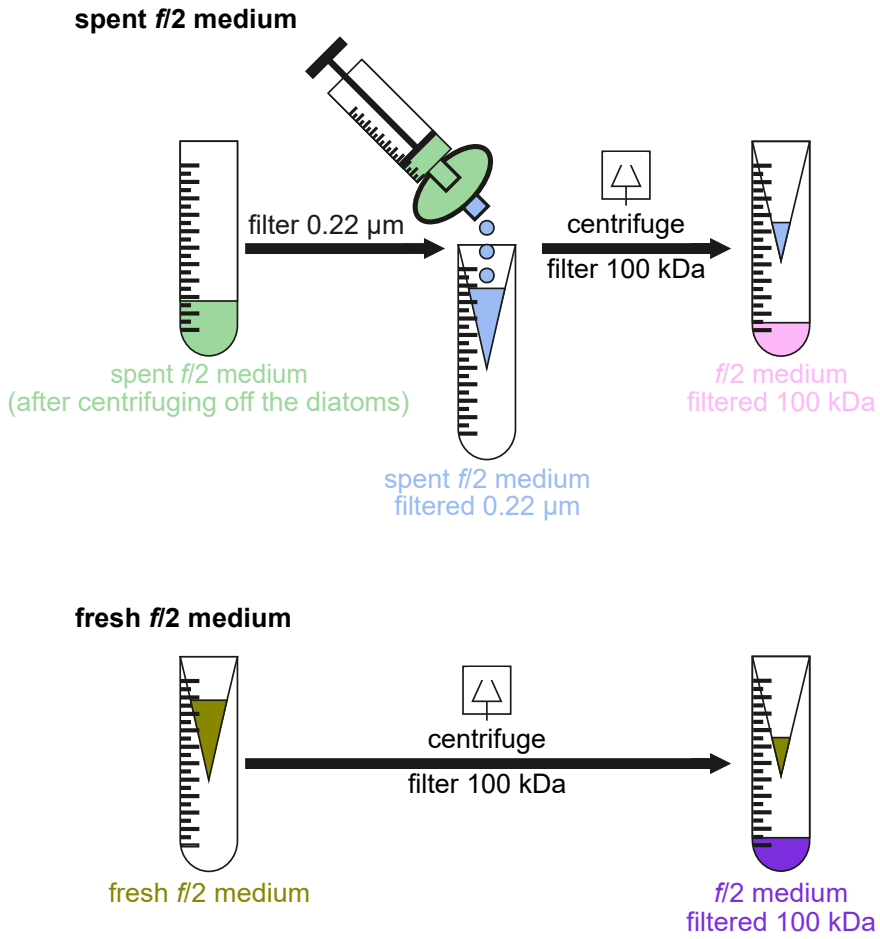

Figure S2: Sample preparation for the ice nucleation experiments with the *f*/2 medium. The spent medium should only contain a few diatoms, because the diatoms were separated from the medium by centrifugation before (green vial). By filtration with a syringe-filter, we removed the remaining cells and retained smaller *F. cylindrus* fragments and the *fc*IBP in the filtrate (blue solution). The solution was filtered by centrifugation filtration and the resulting filtrate should only contain soluble macromolecules smaller than 100 kDa, e.g. *fc*IBP (pink vial). The fresh *f*/2 medium (olive solution) does not contain any cells, fragments or *fc*IBP and was also filtered by centrifugation filtration as a reference (purple vial).

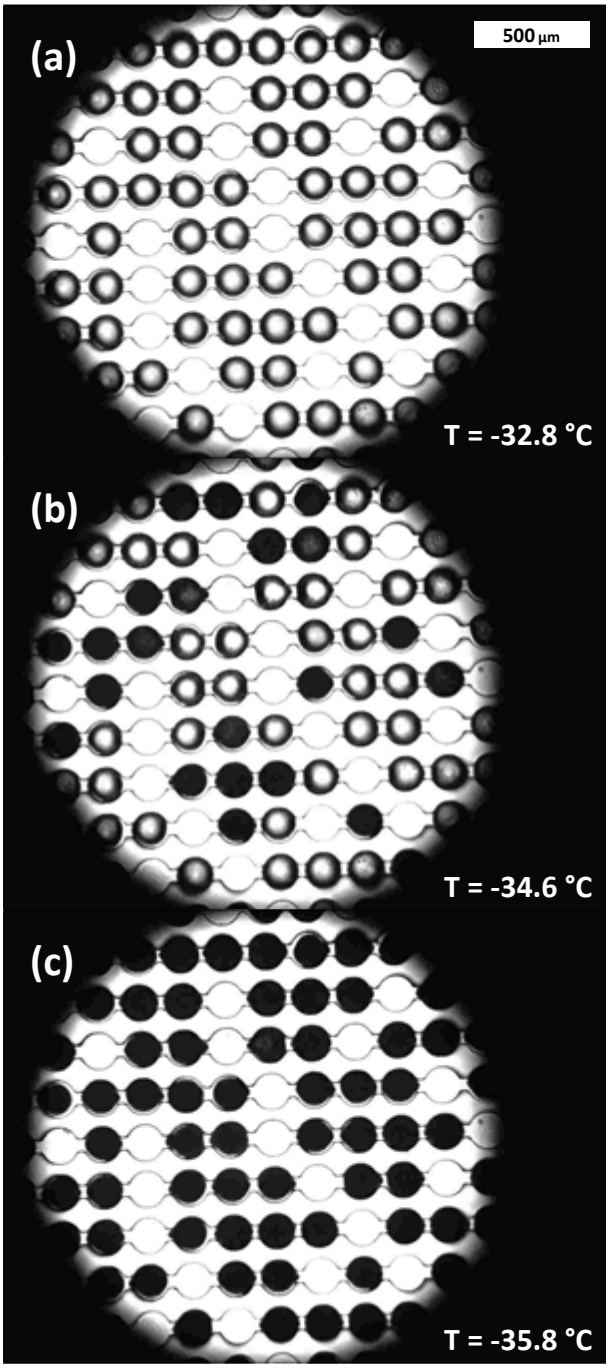

Figure S3: Optical photomicrographs of the freezing of microfluidic droplets during one of three freezing experiments with unfiltered *F. cylindrus* suspensions in artificial seawater (concentration of 2×10^6 cells mL^{-1}). The white scale bar in the top left indicates a length of 500 µm and is the same for all three images. The droplets' diameter is about (90 ±5) µm. **a:** At a temperature of -32.8 °C all droplets are still liquid. This is the last picture before the freezing of the first droplet during this experiment. **b:** At a temperature of -34.6 °C some droplets are already frozen (black), while other droplets are still liquid (white). **c:** At a temperature of -35.8 °C all droplets are frozen. This is the first picture after the freezing of the last droplet in this experiment.

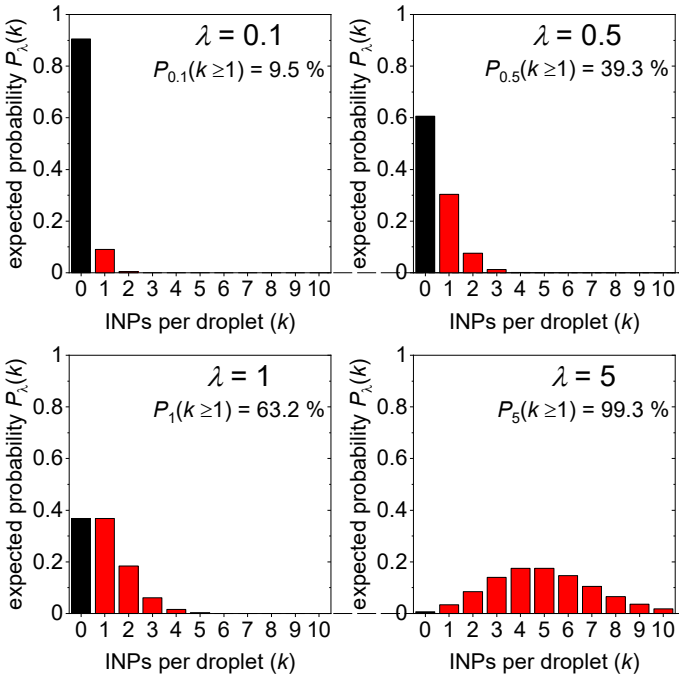

Figure S4: Calculated probability $\boldsymbol{P_\lambda(k)}$ of the number $\boldsymbol{k}$ of INPs per droplet for different values $\boldsymbol{\lambda}$ of the average cell concentration per droplet. The black-coloured bars indicate the probability for the occurrence of droplets without any INPs, while the red-coloured bars indicate the combined probability $\boldsymbol{P_\lambda(k \geq 1)}$ for droplets containing at least one INP. The corresponding values for $\boldsymbol{P_\lambda(k \geq 1)}$ are annotated in each panel for different values of $\boldsymbol{\lambda}$.

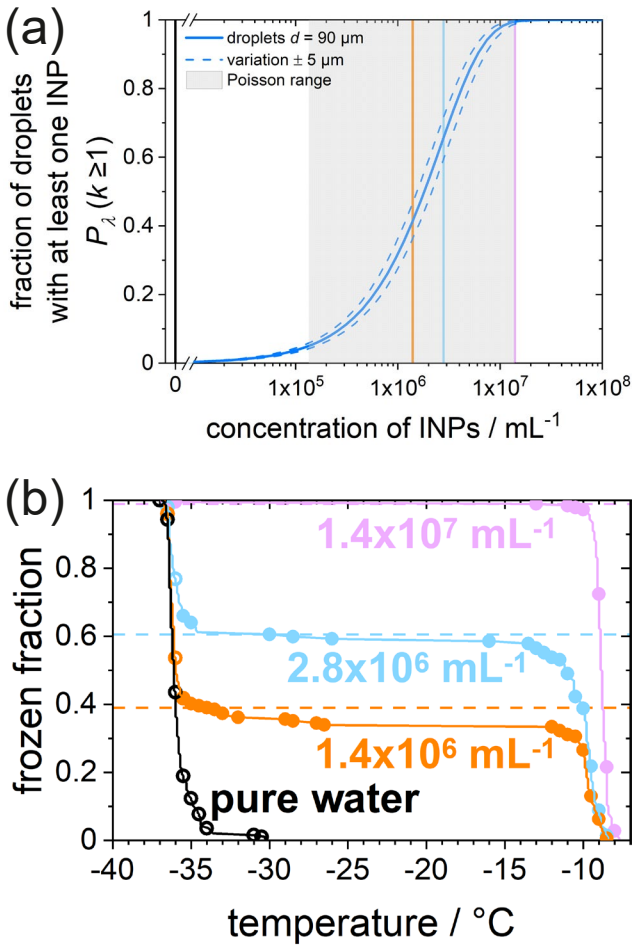

Figure S5: (a) Fraction of droplets containing at least one INP, $\boldsymbol{P_\lambda(k \geq 1)}$ as a function of INP concentration in the investigated *P. syringae* sample. The solid blue curve represents the values of $\boldsymbol{P_\lambda(k \geq 1)}$ for the droplets in the WISDOM experiment with a diameter of 90 µm, calculated using Eq. (S7), the dashed curves indicate the uncertainty for a variation of ±5 µm in droplet diameter. The grey shaded area shows the Poisson relevant range, with the lower and upper limits at the concentrations corresponding to $\boldsymbol{P_\lambda(k \geq 1)}$ = 0.050 and $\boldsymbol{P_\lambda(k \geq 1)}$ = 0.995, respectively. The coloured vertical bars mark the experimentally investigated concentrations of *P. syringae*: 1.4 x 10^6 mL^{-1} (orange), 2.8 x 10^6 mL^{-1} (blue), and 1.4 x 10^7 mL^{-1} (purple) and pure water (black). A comparable plot for the *F. cylindrus* diatoms can be found in Fig. S6. **(b)** Fraction of frozen droplets as a function of temperature for different concentrations of *P. syringae* bacteria in double-distilled water (coloured) and pure double-distilled water (black) for reference. The horizontal lines mark the values for $\boldsymbol{P_\lambda(k \geq 1)}_{\text{measured}}$, see text. Data points of frozen fractions are binned in temperature intervals of 0.5 °C (intervals without freezing events are not shown). Filled circles represent droplets containing *P. syringae* cells (based on calculations for $\boldsymbol{P_\lambda(k \geq 1)}$ with Eq. (S7)), in which freezing was induced heterogeneously. Open circles represent droplets that should not contain *P. syringae* according to the calculations and, thus froze homogenously.

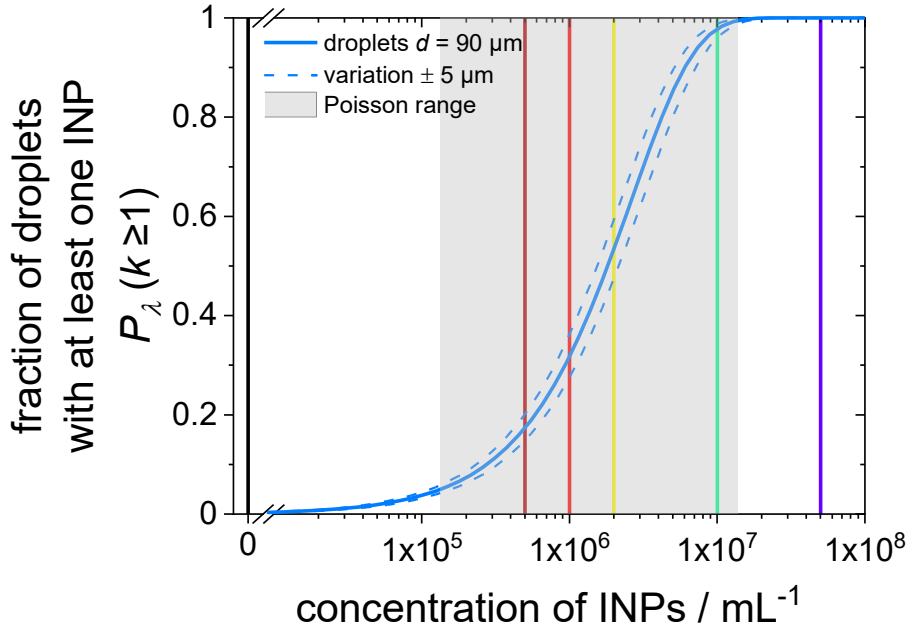

Figure S6: Fraction of droplets with at least one INP, $\boldsymbol{P_\lambda(k \geq 1)}$, as a function of INP concentration in the investigated samples. The solid blue curve represents the values of $\boldsymbol{P_\lambda(k \geq 1)}$ for the droplets in the microfluidic experiment with a diameter of 90 µm. The dashed curves indicate the values for a variation of ±5 µm in droplet diameter, i.e. 85-95 µm. The calculations of these curves are based on Eq. (S7). The grey shaded area shows the Poisson relevant range, see main text for definition, with the lower and the upper limits at the INP concentrations corresponding to $\boldsymbol{P_\lambda(k \geq 1)}$ = 0.050 and $\boldsymbol{P_\lambda(k \geq 1)}$ = 0.995. The vertical bars mark the concentration of the *F. cylindrus* diatom suspensions used in the experiments: 5×10^5 mL^{-1} (dark red), 1×10^6 mL^{-1} (bright red), 2×10^6 mL^{-1} (yellow), 1×10^7 mL^{-1} (green) and 5×10^7 mL^{-1} (purple) and pure seawater (black).

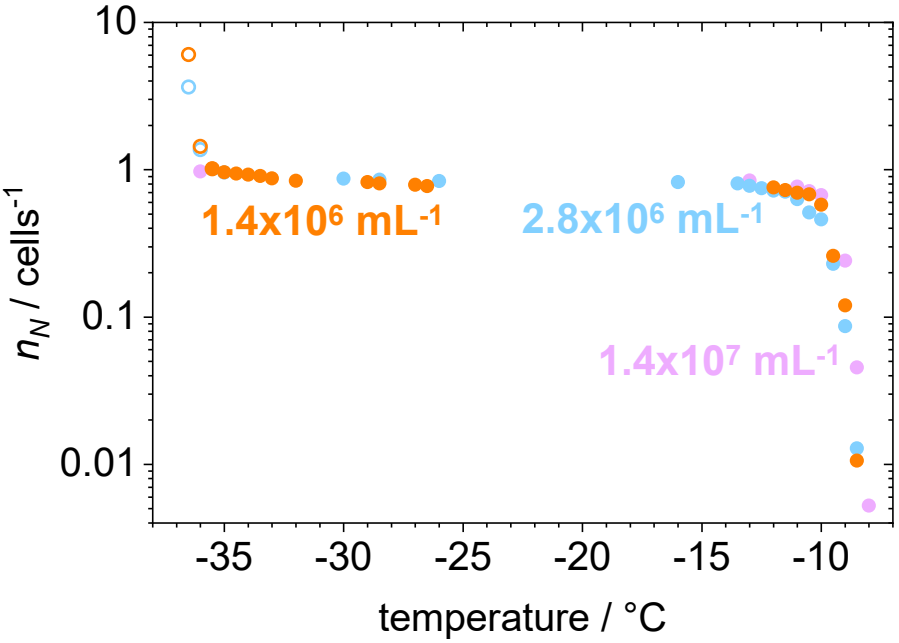

Figure S7: Cumulative number of ice nucleating active sites, $\boldsymbol{n_N}$, for three different *P. syringae* bacteria suspensions with colours indicating the respective concentration. Filled circles represent droplets containing bacteria, as calculated from Eq. (S7), while open circles represent droplets devoid of INP.

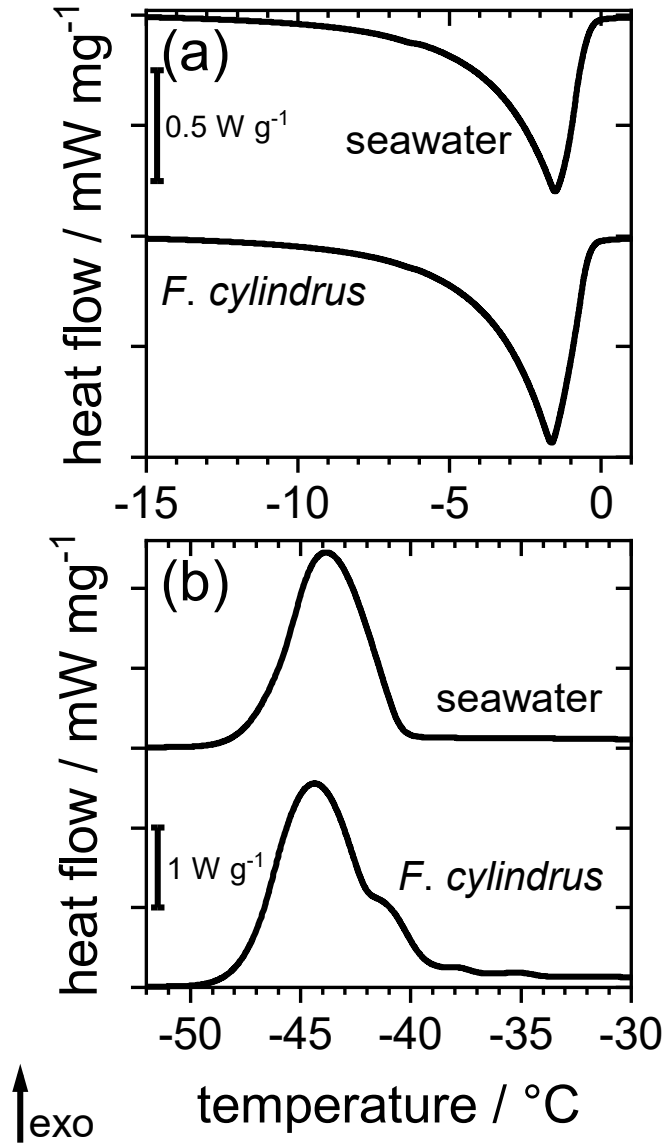

Figure S8: Comparison of DSC thermograms of water-in-oil emulsions containing pure artificial seawater and artificial seawater with *F. cylindrus* cells. **(a)** The endothermic melting-signals are almost identical for pure seawater and seawater containing diatoms. **(b)** Exothermic freezing signals for pure seawater and seawater containing diatoms. While the seawater emulsion shows only one freezing signal, the emulsion containing *F. cylindrus* shows the same signal but with a shoulder and smaller signals at higher temperature, indicative of diatom-induced heterogeneous ice nucleation.

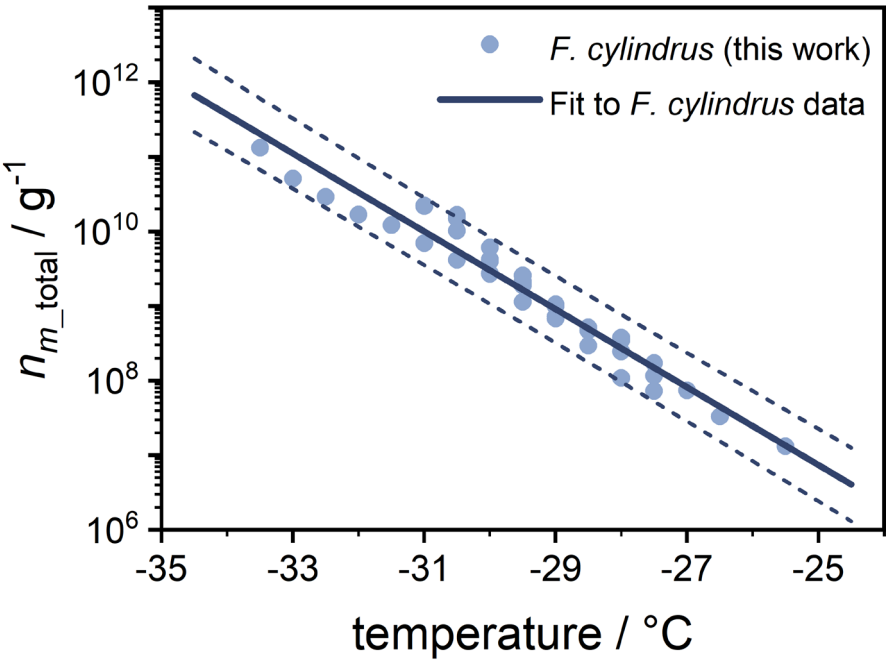

Figure S9: Measured values for $\boldsymbol{n_{m\_total}}$ of *F. cylindrus* diatoms. The solid line represents a fit of the experimental $\boldsymbol{n_{m\_total}}$ values (blue symbols) for the *F. cylindrus* diatoms. The parameterization of the fit is given in Eq. (S10). The dotted lines indicate to the upper and lower 2σ prediction bands of this fit. The temperatures are corrected for the freezing point depression of artificial seawater and, thus, represent ice nucleation temperatures in pure water.

References

Budke, C. and Koop, T.: BINARY: an optical freezing array for assessing temperature and time dependence of heterogeneous ice nucleation, Atmos. Meas. Tech., 8, 689–703, doi:10.5194/amt-8-689-2015, 2015.

Dreischmeier, K., Budke, C., Wiehemeier, L., Kottke, T., and Koop, T.: Boreal pollen contain ice-nucleating as well as ice-binding 'antifreeze' polysaccharides, Scientific reports, 7, 41890, doi:10.1038/srep41890, 2017.

Eickhoff, L., Dreischmeier, K., Zipori, A., Sirotinskaya, V., Adar, C., Reicher, N., Braslavsky, I., Rudich, Y., and Koop, T.: Contrasting Behavior of Antifreeze Proteins: Ice Growth Inhibitors and Ice Nucleation Promoters, The journal of physical chemistry letters, 10, 966–972, doi:10.1021/acs.jpclett.8b03719, 2019.

Gute, E. and Abbatt, J. P.: Ice nucleating behavior of different tree pollen in the immersion mode, Atmospheric Environment, 231, 117488, doi:10.1016/j.atmosenv.2020.117488, 2020.

Koop, T., Luo, B., Biermann, U. M., Crutzen, P. J., and Peter, T.: Freezing of HNO3/H2SO4/H2O Solutions at Stratospheric Temperatures: Nucleation Statistics and Experiments, J. Phys. Chem. A, 101, 1117–1133, doi:10.1021/jp9626531, 1997.

Koop, T. and Murray, B. J.: A physically constrained classical description of the homogeneous nucleation of ice in water, The Journal of chemical physics, 145, 211915, doi:10.1063/1.4962355, 2016.

Morris, C. E., Sands, D. C., Bardin, M., Jaenicke, R., Vogel, B., Leyronas, C., Ariya, P. A., and Psenner, R.: Microbiology and atmospheric processes: research challenges concerning the impact of airborne micro-organisms on the atmosphere and climate, Biogeosciences, 8, 17–25, doi:10.5194/bg-8-17-2011, 2011.

Murray, B. J., O'Sullivan, D., Atkinson, J. D., and Webb, M. E.: Ice nucleation by particles immersed in supercooled cloud droplets, Chemical Society reviews, 41, 6519–6554, doi:10.1039/c2cs35200a, 2012.

Reicher, N., Segev, L., and Rudich, Y.: The WeIzmann Supercooled Droplets Observation on a Microarray (WISDOM) and application for ambient dust, Atmos. Meas. Tech., 11, 233–248, doi:10.5194/amt-11-233-2018, 2018.

Wex, H., Augustin-Bauditz, S., Boose, Y., Budke, C., Curtius, J., Diehl, K., Dreyer, A., Frank, F., Hartmann, S., Hiranuma, N., Jantsch, E., Kanji, Z. A., Kiselev, A., Koop, T., Möhler, O., Niedermeier, D., Nillius, B., Rösch, M., Rose, D., Schmidt, C., Steinke, I., and Stratmann, F.: Intercomparing different devices for the investigation of ice nucleating particles using Snomax ® as test substance, Atmos. Chem. Phys., 15, 1463–1485, doi:10.5194/acp-15-1463-2015, 2015.

Xi, Y., Mercier, A., Kuang, C., Yun, J., Christy, A., Melo, L., Maldonado, M. T., Raymond, J. A., and Bertram, A. K.: Concentrations and properties of ice nucleating substances in exudates from Antarctic sea-ice diatoms, Environmental science. Processes & impacts, 23, 323–334, doi:10.1039/d0em00398k, 2021.